Article:
Abdullah, NA, Curiel-Sosa, JL, Taylor, ZA et al. (2017) Transversal crack and delamination of laminates using XFEM. Composite Structures, 173. pp. 78-85. ISSN: 0263-8223

https://doi.org/10.1016/j.compstruct.2017.04.011

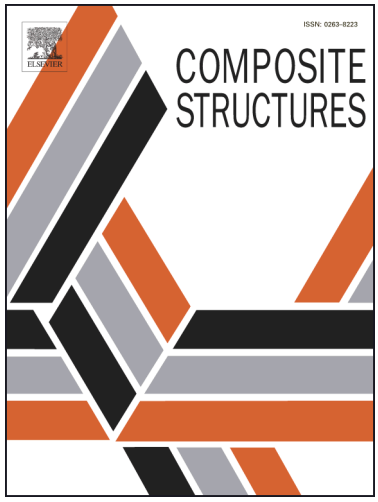

Transversal crack and delamination of laminates using XFEM

Nur Azam Abdullah, Jose Luis Curiel-Sosa, Zeike A. Taylor, Behrooz Tafazzolimoghaddam, J.L. Martinez Vicente, Chao Zhang

PII: S0263-8223(16)32851-3
DOI: http://dx.doi.org/10.1016/j.compstruct.2017.04.011
Reference: COST 8442

To appear in: *Composite Structures*

Received Date: 13 December 2016
Accepted Date: 6 April 2017

Please cite this article as: Abdullah, N.A., Curiel-Sosa, J.L., Taylor, Z.A., Tafazzolimoghaddam, B., Martinez Vicente, J.L., Zhang, C., Transversal crack and delamination of laminates using XFEM, *Composite Structures* (2017), doi: http://dx.doi.org/10.1016/j.compstruct.2017.04.011

Transversal crack and delamination of laminates using XFEM

Nur Azam Abdullah[a,b,*], Jose Luis Curiel-Sosa[a,], Zeike A. Taylor[a,], Behrooz Tafazzolimoghaddam[a,], J.L Martinez Vicente[c,], Chao Zhang[d,]

[a]*Department of Mechanical Engineering, The University of Sheffield, Sir Frederick Mappin Building, Mappin Street, S1 3JD Sheffield, United Kingdom*

[b]*Department of Mechanical Engineering, International Islamic University Malaysia, Malaysia*

[c]*Escuela Técnica Superior de Ingenieros Industriales de Ciudad Real, Universidad de Castilla-La Mancha, Departamento de Mecánica Aplicada e Ingeniería de Proyectos, INEI Avenida Camilo José Cela s/n, 13071 Ciudad Real, Spain*

[d]*School of Mechanical Engineering, Jiangsu University, Zhenjiang, China*

Abstract

This paper offers a new insight into the computational modelling of crack and delamination of carbon fiber composite. Both transversal cracks (intralaminar) and delamination (interlaminar) are modelled with Extended Finite Element Method (XFEM). Constitutive and fracture laws are integrated to model the initiation of crack or delamination, and their subsequent evolution. The study includes the size effect assessment of composite due to the increment of composite thickness. The results are in close agreement between the experimental and analytical data of each specimen modelled based on the size of the carbon fiber composite volume.

Keywords: crack, delamination, size effect, composite, finite element modelling, fracture.

1. Introduction

The computational modelling of the fracture study of crack and delamination of composite structure is still under development. Several assumptions and techniques have been developed in this field of study to obtain numerically accurate damage predictions. To simulate an accurate crack propagation, the modelling method requires a reliable calculation of the stress intensity factor (SIF) to be able to apply fracture criteria [1]. Al-ansari et al. [2], Lecheb et al. [3] and Zhou et al. [4] studied the stress intensity factor for 2-dimensional (2D) form composite structure. FEM's and meshfree method were compared to calculate the SIF for the Mode I fracture [2]. XFEM is used to estimate the SIF in Mode I and Mode II crack problems [3]. One of the reported advantages of XFEM is that it allows both Mode I and Mode II modelling straightforwardly through convenient criteria. The study found that the composite crack angle imposing a minimal SIF.

The extended finite element method (XFEM) was developed by Ted Belytschko and collaborators in 1999 to solve structural crack propagation problems without continuous or minimum re-meshing [5]. Mode II fracture propagation modelling using XFEM in concrete with the additive material of siliceous fly-ash was presented by Golewski et al. [6]. The 2D crack numerical modelling using XFEM showed good agreement with the experimental data.

Developments in XFEM are still in progress as pointed out by Huynh and Belytschko [7]. They focused on the material interfaces where the crack tip enrichments and computational meshes were assigned. The method applied is used to solve both 2D and 3D composite structure cracks [7]. In the standard FEM, the element edges coincide with the material interfaces and the required crack surfaces, whereas XFEM has eliminated this restriction. Some researches that related to the crack propagation of 3D composite structures using XFEM in Abaqus can be seen in Moreno et al. [8] and Navarro-Zafra et al. [9]. Both works showed the modelling of intralaminar cracks without any interlaminar crack involved.

*Corresponding author

Email addresses: nababdullah1@sheffield.ac.uk (Nur Azam Abdullah), j.curiel-sosa@sheffield.ac.uk (Jose Luis Curiel-Sosa)

URL: http://www.jlcurielsosa.org (Jose Luis Curiel-Sosa)

Some works that related to the modelling of delamination in composite structures used integrated XFEM and cohesive elements [10]; [11]; [12]; [13]. Grogan et al. [10] applied a combination of XFEM and cohesive elements to simulate microcrack nucleation in composite structures. The random microcrack and propagation (intralaminar failure) were computed based on XFEM while the delamination between plies was computed based on a mixed mode surface cohesive zone model (SCZM). Yazdani et al. [11] applied the XFEM to model the composite mixed-mode delamination. The adhesive contacts were modelled between each layer with cohesive elements. The computation interlaminar stresses were established based on a first-order shear deformation theory. The interlaminar stresses increment was triggered by the Poissons ratios mismatch and interaction which led to the delamination initiation. It is clear that the combined crack and delamination modelling is still under development.

Hu et al. [12] defined three cases to establish the matrix fracture and delamination migration based on a progressive damage model. For each case, laminates were tested with distinct staking sequences. Crack initiation was based on the expected crack angle path (pre-allocation) for each layer of composite. The delamination by cohesive elements was not triggered until the matrix crack touched the interface, which is a step forward with respect to Hallet et al. [14], in which every crack was initially pre-allocated.

In this paper, a step forward has been given in the simulation by doing both intralaminar and interlaminar fracture by XFEM. The numerical computational presented in this paper is to develop the transversal crack and delamination of carbon fiber composite.

2. Extended Finite Element Modelling

In this present work, the elements in the interface (SOLID) are subjected to splitting by enrichment (XFEM) and the initiation criteria as well as evolution criteria based on energy release rate.

2.1. Crack propagation using Level Set Method

The application of the level set method for solving the fracture problem is difficult in constraining the evolution of the signed distance function during crack propagation while maintaining the existing crack surface in a frozen state [15]. Several modifications have been made since the level set method was implemented in open curve interfaces such as cracks. Instead of only one set level which is denoted by ϕ, the second set level of ψ is also required at the crack tip.

The zero-level set of function $\psi(x,t)$ is used to simplify a 1D crack growth. The intersection of the zero-level set of function $\psi(x,t)$ with the zero-level set of function $\phi^k(x,t)$ is set at the end point of the crack where k is the number of tips at the defined crack. An assumption is made for a condition where ψ is orthogonal to ϕ. The nodes are only used as storages for level set function values.

$$\phi_{,i}\psi_{,i} = 0 \tag{1}$$

Using the similar finite element shape function, the functions are interpolated over the mesh in which the function can now be written as in Equation 2 and Equation 3.

$$\phi^k(x,t) = \sum_{j=1}^{n} N_j(x)(\phi^k(x,t)_j) \tag{2}$$

$$\psi(x,t) = \sum N_j(x)(\psi_j(x,t)) \tag{3}$$

However, the zero level set of ψ is cut through the entire domain even when the crack is actually embedded inside a domain. An assumption of the part is fixed without changing any shape or moving once the crack has emerged. The iteration updates of ϕ^k and ψ functions lead to the recalculation of the ϕ function, which are used to model the crack growth. The crack growth direction of θ is the factor of ϕ^k and ψ evolutions. The velocity vector $\mathbf{v} = (\mathbf{v}_x, \mathbf{v}_y)$, which is always normal to the interfaces, is determined for every step with the displacement of the crack tip.

The procedure of level set function of ϕ_n^k and ψ_n evolutions in the n- step was simplified [16]. The level set rotation of ϕ_n^k is expressed by $\phi_n^{k,r}$ and computed based on 4 and $\psi_{(n+1)}$ in Equation 5;

$$\phi_n^{k,r} = (x - x_k)\frac{\mathbf{v}_x}{\|\mathbf{v}\|} + (y - y_k)\frac{\mathbf{v}_y}{\|\mathbf{v}\|} \tag{4}$$

where x is the nodal coordinate and x_k is the crack tip coordinate.

$$\psi_{n+1} = \left|(x - x_k)\frac{\mathbf{v}_x}{\|\mathbf{v}\|} + (y - y_k)\frac{\mathbf{v}_y}{\|\mathbf{v}\|}\right| \tag{5}$$

Next, the updated crack tip location is calculated based on Equation 6.

$$\phi_{n+1}^{k} = \phi^{k,r} - \Delta t \, \|\mathbf{v}\| \tag{6}$$

Abaqus/Standard software does not estimate the exact and real time of the test to be performed as it is a Newton - Raphson solver and hence iterations are computed without time step. This is the reason where the implementation of velocity in Equation 6 was introduced [17]. The velocity is multiplied with the time difference (Δ t) to calculate the increment iteration in this simulation. Therefore, the velocity parameter is used to estimate the displacement (crack propagation) on the surface of the composite.

Equation 7 is used for more than one crack tip.

$$\phi(x,t) = \max_{k}(\phi^{k}) \tag{7}$$

Lastly, the intersection of zero level sets of ϕ_{n+1}^{k} and ψ_{n+1} is computed to solve the location of new crack tip of k. Figure 1 shows the crack tip deformation field coordinates and typical contour Γ [18]. The polar coordinates of r and θ with respect to the tangential of crack tip at a point x can be written as shown in Equation 8 and Equation 9.

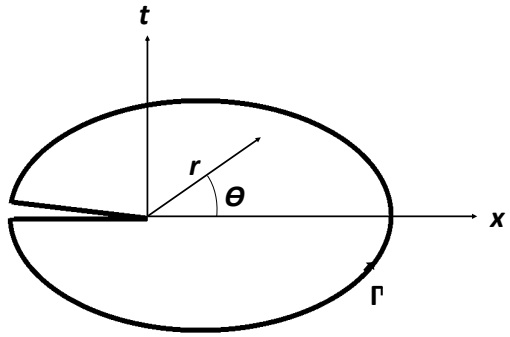

Figure 1: Crack tip deformation field coordinates and typical contour Γ

$$r = \sqrt{\phi(x,t)^2 + \psi(x,t)^2} \tag{8}$$

$$\theta = tan^{-1}[\frac{\psi(x,t))}{\phi(x,t))}] \tag{9}$$

By implementing the local coordinate in this analysis, XFEM is used to estimate the crack propagation in the contour region.

2.2. Enrichment Function

The enrichment function is used to solve the discontinuity within the element by providing an additional shape function. Equation 10 shows the approximate displacement applied in the most standard finite element methods, where $N(x)$ is the shape function and d is the change of displacement in every node.

$$u(x) = \sum_{j=1}^{n} N_j(x) d_j \tag{10}$$

To calculate the crack propagation path, some enrichments might be added as shown in Equation 11. The shape function in the second term is added as the enrichment for solving the extra degree of freedom node, which is expressed as a_j with m as the nodes enriched by the Heaviside function. However, for solving the crack at the crack tip, a third notation is required. As the last point of the crack tip is in a singular point form, the $F(x)$ function is used in terms of the singular point radius, where mt is the number of nodes enriched by crack tip asymptotic field enrichments.

Several assumptions and techniques have been developed in this field of study to obtain the accurate damage prediction numerically.

$$u^{h}(x) = \sum_{j=1}^{n} N_j(x) d_j + \sum_{j=1}^{m} N_h(x) H(x) a_j + \sum_{k=1}^{mt} N_k(x) \left[\sum_{l=1}^{mf} F(x) b_k \right] \tag{11}$$

2.3. Damage Initiation

In this paper, maximum principal stress failure criteria are used to predict intralaminar damage initiation as shown in Equation 12;

$$\sigma_{1,2} = \frac{\sigma_x + \sigma_y}{2} \pm \sqrt{\frac{(\sigma_x - \sigma_y)^2}{2} + \tau_{xy}^2} \tag{12}$$

$$tan2\theta_p = \frac{2\tau_{xy}}{\sigma_x - \sigma_y} \tag{13}$$

A damage occurs if any of these stress components such as σ_1,σ_2,τ_{12} in the principal material axis meet the criteria as given in Equations 14, 15 and 16.

$$\sigma_1 \geq \begin{pmatrix} \sigma_1^{T*}(\sigma_1>0) \\ -\sigma_1^{C*}(\sigma_1<0) \end{pmatrix} \tag{14}$$

$$\sigma_2 \geq \begin{pmatrix} \sigma_2^{T*}(\sigma_2>0) \\ -\sigma_2^{C*}(\sigma_2<0) \end{pmatrix} \tag{15}$$

$$\tau_{12} \geq \tau_{12}^* \tag{16}$$

where σ_1^{T*} is the longitudinal tensile strength, σ_1^{C*} is the longitudinal compressive strength, σ_2^{T*} is the transverse tensile strength, σ_2^{C*} is the transverse compressive strength and τ_{12}^* is the in-plane shear strength.

The standard formulation in Equation 12 is modified for anisotropic mixed mode crack maximum principal of stress as presented in Equation 17 [19].

$$\sigma_{max} = \frac{\sigma_{11} + \sigma_{22}}{2} \pm \sqrt{\frac{(\sigma_{11} - \sigma_{22})^2}{2} + \tau_{12}^2} \tag{17}$$

Each ply will fail based on the material properties assigned in terms of either tension or compression, following the maximum stress failure envelope. During the tensile test simulation, if the ply meets any of the above-mentioned conditions, then the ply fails.

2.4. Damage Evolution

The mixed mode in crack propagation leads to the formation of cracks and delamination. The non-zero K_I and K_{II} stress intensity factors are established because of the inclined or curvilinear propagations from multiaxial loadings. These two stress intensity factors emerged when a notch or a crack was subjected to in-plane loading [19].

Both stress intensity factors for an inclined crack can be written as in Equation 18 and Equation 19, where a is the crack length and θ_0 is the angle between the crack inclination and the existing crack.

$$K_I = \sigma \sin^2 \theta_0 \sqrt{a\pi} \tag{18}$$

$$K_{II} = \sigma \sin \theta_0 \cos \theta_0 \sqrt{a\pi} \tag{19}$$

The relationship between the stress intensity factors and the strain energy release rate based on the crack growth is defined in Equation 20:

$$G = G_I + G_{II} = \frac{{K_I}^2}{E_I'} + \frac{{K_{II}}^2}{E_{II}'} \tag{20}$$

where E_I' and E_{II}' are generalised elastic modulus.

Nucleation is not intended, rather an initiation via Equation 14 and Equation 15 together with delamination evolution through energy release criterion is used. For this reason, Equation 21 is provided where G_c is the critical fracture toughness.

$$G \geq G_c \tag{21}$$

Based on the maximum energy release rate, both these stress intensity factors can be expressed in θ from Figure 1 as given in Equation 22 and Equation 23.

$$K_I(\theta) = g(\theta) K_I cos\theta + \frac{3}{2} K_{II} sin\theta \tag{22}$$

$$K_{II}(\theta) = g(\theta) K_{II} cos\theta + \frac{3}{2} K_I sin\theta \tag{23}$$

where,

$$g(\theta) = (\frac{4}{3 + cos^2\theta})(\frac{1 - \frac{\theta}{\pi}}{1 + \frac{\theta}{\pi}})^2 \tag{24}$$

3. Fracture Model

This section aims to achieve two objectives. The first part is to demonstrate the crack propagation with delamination simulation using XFEM and the second part is to study the size effect of carbon fiber composite laminates based on the same ply orientation blocked together.

In the first part, the experimental procedure for carbon fiber composite fracture by Hallet et al. [14] is studied. The computational modelling procedure for the same carbon fiber composite specimens used in Ref. [14] is performed using the ABAQUS/standard commercial software. The results are compared for validation so that the modelling procedure gives accurate results based on the maximum principal stress criterion.

For the second part, the modelling of size effect study is performed based on experimentation by Wisnom et al. [20]. They applied the same composite material from Ref. [14] but they have increased the specimen volume thickness to study the size effect experimentally.

3.1. Crack and delamination simulation using XFEM in ABAQUS/Standard

In this section, the carbon epoxy composite plate based on the specimen developed in Hallett et al. [14] was studied where an experiment to estimate the fracture strength of the material due to tensile loading was performed. The material properties of the carbon fiber composite used in the simulation are given in Table 1. The lay-up of the laminate used in this section is $(45/90/-45/0)_s$.

Table 1: Carbon fiber composites elastic properties used in the XFEM analysis

Parameter	Value
E_1	161 GPa
$E_2 = E_3$	11.38 GPa
$G_{12} = G_{13}$	5.17 GPa
G_{23}	3.98 GPa
$v_{12} = v_{13}$	0.32
v_{13}	0.436

Hallett et al. [14] has made a good comparison between the experimentation and the simulation. This is due to the pre-allocations of fracture propagation. The authors have performed a similar experimental tensile test as been done by Ref. [14] to assess the fracture behaviour on the composite plate. The fracture mechanism shown in Figure 2 observed is similar to the one assesed by Ref. [14], i.e transversal crack eventually triggering delamination.

In this research, the specimen of Case 1 is modelled symmetrically with the neutral axis of the composite structure as the symmetrical axis. Each ply of the laminate is modelled as solid element subjected to splitting in the corresponding loading condition. In this work, the symmetrical axis is defined on the top of 0^0 ply at the instance to optimise the structural thickness ratio with the thin crack initiation. The modelling specimen illustration for this analysis is presented in Figure 3. The crack initiation for this model is defined in the middle of the specimen at the bottom at 45^0 inclination. This crack initiation is shown in Figure 3, where it is represented as the rectangular black inside the red dotted line. Boundary conditions are such force motion in traction direction is allowed and transversal motion is not impeded. The crack will propagate based on the damage model and the boundary condition assigned, with no crack path assigned manually.

The length of the specimen in Case 1 is modelled without the grip to reduce the calculation time required for a larger size specimen. The displacement load and fixed boundary condition are applied directly to the end nodes and pulled under tensile loading.

The maximum stress criterion and the energy damage evolution are specified as the damage model for this static analysis. All composite layers with different ply angles and epoxy matrix damage criterion modelling data are obtained from [21]; [22]; [23].

To demonstrate a crack model with delamination, the epoxy matrix used in the model is assumed to be hardened as a layer between each attaching carbon fiber ply. This assumption is very important as the XFEM always exhibits a crack behaviour based on the damage model of a solid isotropic material. In this analysis, if the crack appears between the composite lamina and causes an interlaminar crack, then the crack is called as delamination.

Figure 4 shows the strain contour for the presented composite plate where the transversal crack (intralaminar) and delamination (interlaminar) fracture had propagated simultaneously. The composite structure is considered a complete failure when the elastic region of the stress-strain relation is at the breaking point.

Figure 5 shows the strain contour for each carbon fiber composite ply as the crack and delamination are presented. Figure 5 (a) shows the transversal crack for the ply inclined at 45^0 where the crack is initiated in the middle of the ply. As the transversal crack propagates along the ply, the crack also propagates to the upper side and triggers the next layer. The resulting situation is shown in Figure 5 (b), where the 90^0 ply consists of some delaminations, and the crack constantly propagates to the next composite layer until the simulation ends.

Figure 6 shows the stress-strain plot for Case 1 until the structure fails. A mesh sensitivity analysis is performed to ensure that the number of elements used in this analysis is acceptable without any convergence

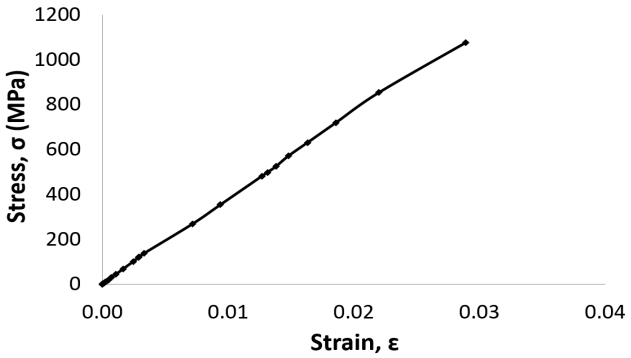

Figure 6: Case 1 - Stress-strain plot

problem. Figure 7 shows the mesh sensitivity analysis for Case 1. The number of elements selected is 6080, for which the failure stress occurred at 1076.36 MPa. The number of elements is selected in such a way that the analysis requires only less computational time. It was observed that the computational failure stress corresponded with the experimental data result consistently, with minimal error.

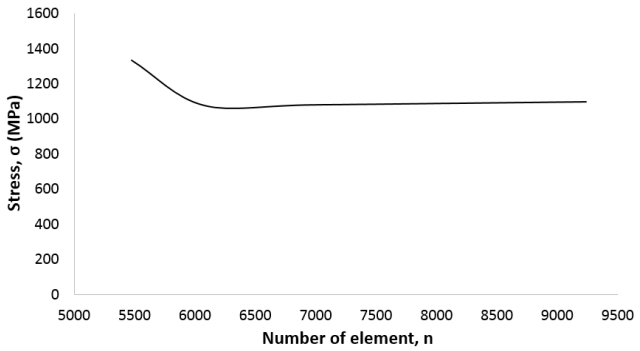

Figure 7: Mesh sensitivity analysis plot

Figure 8 presents the strain contour of Case 1 for the bottom view where the transversal crack and delamination have developed. The bottom view of the transversal crack and delamination is shown in Figure 9, in which the region of both intralaminar and interlaminar crack can be seen clearly. The transversal crack and delamination are in a non-linear form, as the composite structure consists of different orientation angles for each ply. The behaviour of crack propagation for the laminate composite is successfully modelled and is presented in Figure 9 for the bottom view of the composite plate.

3.2. Size effect modelling study on the same ply orientation blocked together

The same material properties of carbon fiber are studied in this section. Wisnom et al. [20] have conducted experiments for investigating the size effect modelling study on the same ply orientation blocked together in carbon fiber composite. $(45_m/90_m/-45_m/0_m)_{ns}$ composite lay-ups are used, where m is the number of same ply orientation blocked together = 1, 2 and 4 and n = 1. These results are termed as the validation for the simulation. Table 4 shows the experimental results presented in Ref. [20] to validate the analytical calculation data. The results are used as a benchmark for the present work.

The objective of this subsection is to study the size effect on the addition of same ply orientation blocked together using a numerical computational technique. The reason is based on Ref. [20]; where they found that the strength of carbon fiber composite became lower when the tensile test was performed on larger volume of carbon fiber composite plate. The strategy was performed by applying some additional plies as shown in the carbon fiber composite lay-up in Table 4, Table 5 and Table 6. Thus; the application of same ply orientation blocked together was the reason that the composite plate strength was reduced even the composite plate volume was bigger.

Table 5 shows the difference in the present work simulation results with the analytical expected strength for each case. The percentage difference increases with a rise in the size of the modelled composite specimen. The present work also compares the results with an experimental data as shown in Table 6.

These results indicate that the size effect assessment of the same ply orientation blocked together in carbon fiber composite is different if it is compared to an isotropic material such as metal. Carbon fiber

composite is one of the anisotropic materials. The mechanical properties are dependent on the fiber angle orientation. In this case, the failure stress decreases as the volume of the carbon fiber composite increases.

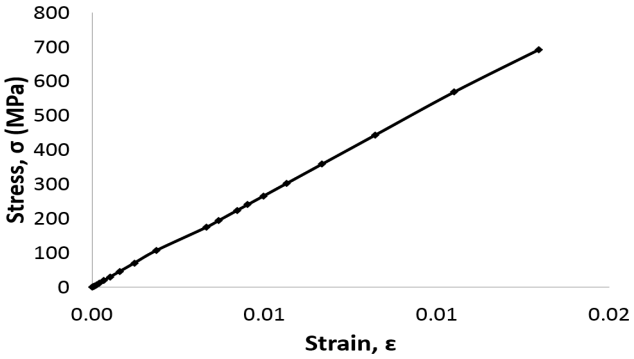

Figure 10: Case 2- stress-strain plot

Figure 10 and Figure 11 show the stress-strain plot of Case 2 and Case 3 respectively; where the volume of the composite structures are bigger than the composite structure of Case 1. As the volume of composite structure in Case 3 is larger than the composite structure of Case 2, the failure stress of Case 3 specimen is found to be lower than the specimen of Case 2.

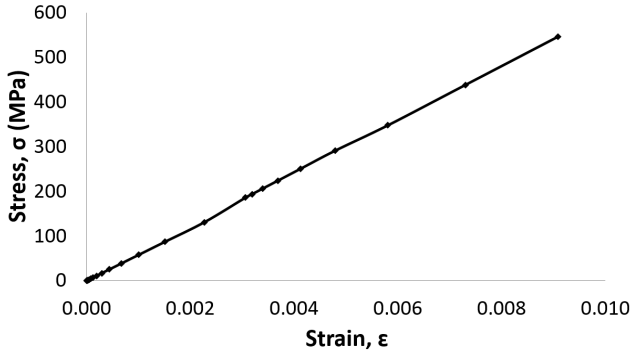

Figure 11: Case 3- stress-strain plot

Graph in Figure 12 shows the comparison of results between the analytical calculation of the failure stress and the experimental data of the failure stress along with the simulation results performed in this report. It is clearly shown that the trend of failure stress nonlinearly reduces with the increment in carbon fiber composite plate volume and failure stress, as presented in Figure 12. The approximate linear of strength reduction in Figure 13 is plotted to examine the effectiveness of XFEM in predicting the size effect phenomenon. From this graph, the size effect mod-

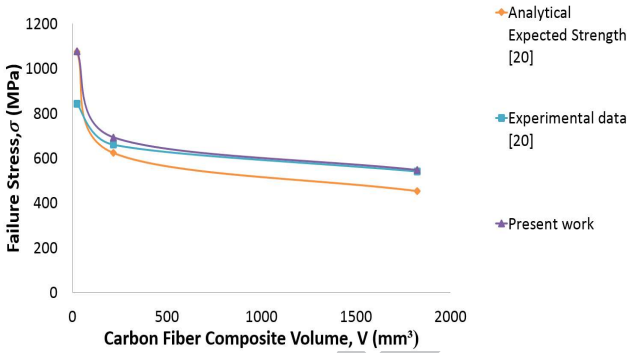

Figure 12: All cases- size effect strength plot

elling of composite using XFEM renders a slightly higher approximation compared to the experimental and expected strength provided by Ref. [20].

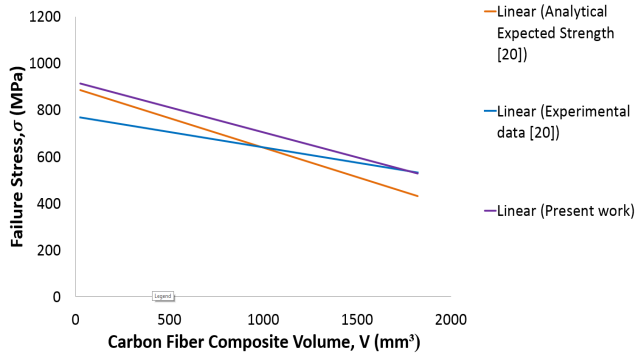

Figure 13: All cases- linear approximation of size effect strength plot

As the composite structure is an anisotropic material, its behaviour is different from the isotropic material where the increment in the size of the isotropic structure increases the failure strength. The trend for simulation results shows a good agreement with the analytical as well as the experimental data.

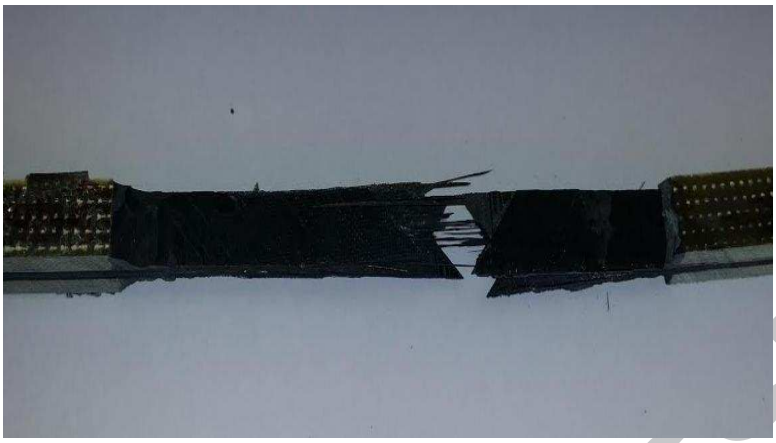

Figure 2: Experimental results of crack and delamination

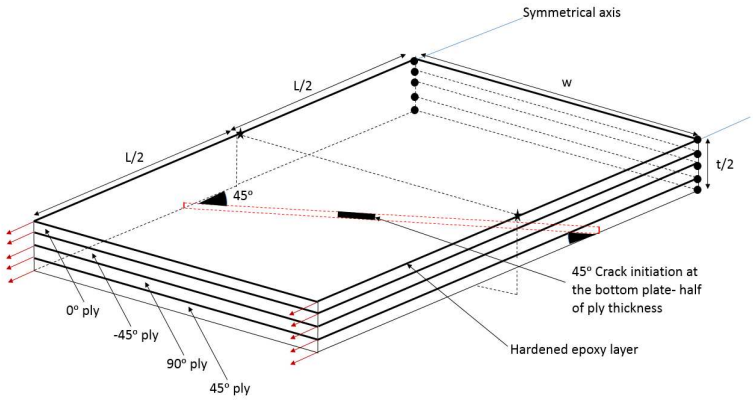

Figure 3: Specimen modelling of Case 1

Table 2: Yield stress used in XFEM analysis taken from Ref. [21] and Ref. [23]

Material	Angle	Maximum principal stress (MPa)
Carbon fiber	0	476
Carbon fiber	45	149
Carbon fiber	90	476
Carbon fiber	-45	149
Epoxy	Nil	50.2

Table 3: Fracture toughness value of carbon fiber composite laminate by Ref. [22] and Ref. [23]

Layer	G_{lc} (kJ/m^2)
Carbon fiber	91.6
Epoxy matrix	1.7

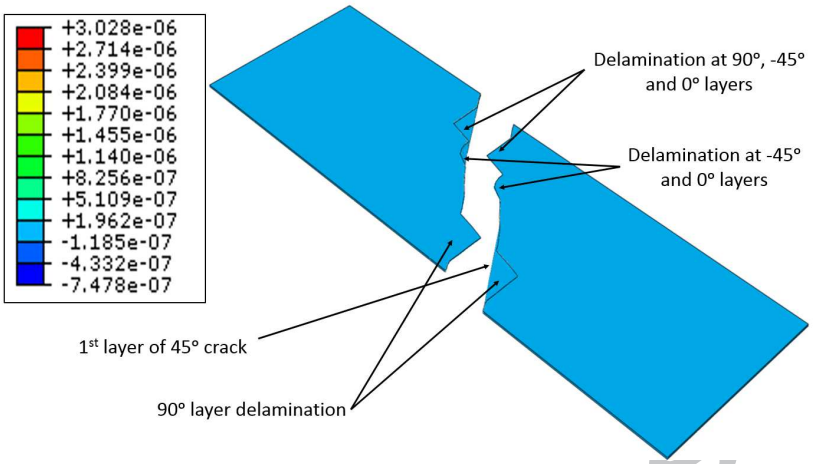

Figure 4: Case 1 - Crack and delamination simulation result [unit:strain]

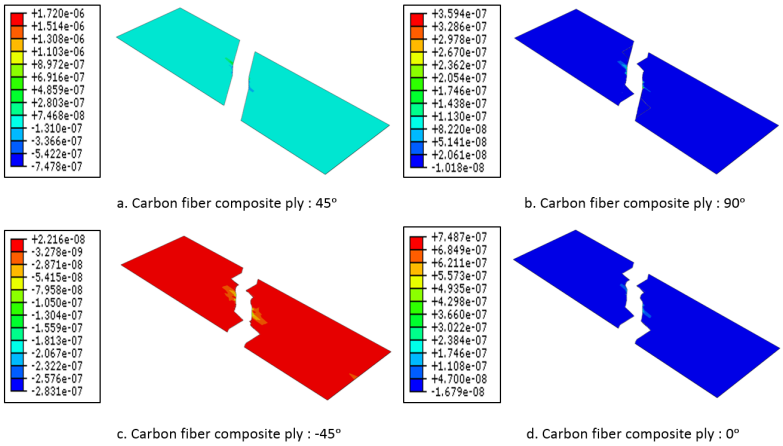

Figure 5: Case 1 - Crack and delamination strain contour for each ply [unit:strain]

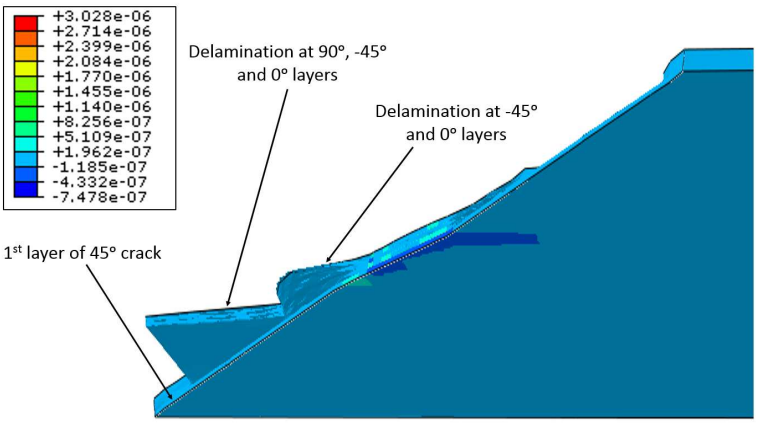

Figure 8: Case 1 - strain contour: Bottom view of transversal crack and delamination at focus area [unit:strain]

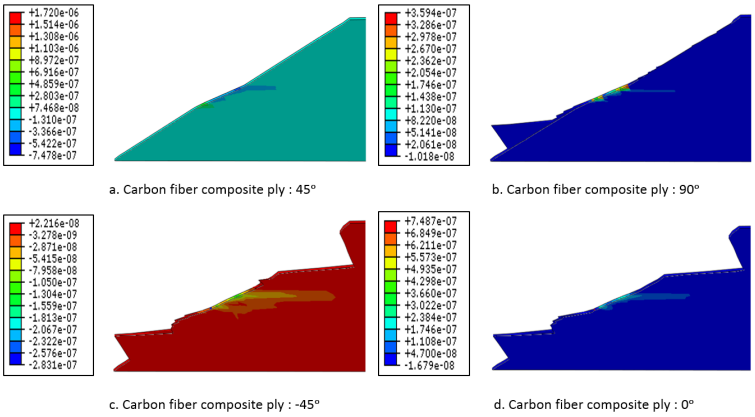

Figure 9: Case 1 - strain contour: Bottom view of transversal crack and delamination per ply at focus area [unit:strain]

Table 4: Percentage difference of expected strength and experimental results [20]

Case	Lay-up	Expected strength (MPa)	Experimental (MPa)	Difference %
1	$(45/90/\text{-}45/0)_s$	1074	842	21.6
2	$(45_2/90_2/-45_2/0_2)_s$	642	660	2.8
3	$(45_4/90_4/-45_4/0_4)_s$	454	541	19.2

Table 5: Percentage difference between the expected strength and failure stress - present work

Case	Lay-up	Expected strength (MPa)[20]	Failure stress-present work (MPa)	Difference %
1	$(45/90/\text{-}45/0)_s$	1074	1076.36	0.2
2	$(45_2/90_2/-45_2/0_2)_s$	642	692.47	7.86
3	$(45_4/90_4/-45_4/0_4)_s$	454	546.59	20.39

Table 6: Percentage difference of experimental and failure stress-present work

Case	Lay-up	Experiment (MPa)[20]	Failure stress-present work(MPa)	Difference %
1	$(45/90/\text{-}45/0)_s$	842	1076.36	27.83
2	$(45_2/90_2/-45_2/0_2)_s$	660	692.47	4.92
3	$(45_4/90_4/-45_4/0_4)_s$	541	546.59	1.03

4. Conclusion

This paper offers a new insight on the computational modelling of crack and delamination of carbon fiber composite. Transversal crack and delamination have been assessed using XFEM validated against experimental and analytical data. Both transversal crack and delamination analysis are simulated using XFEM for a composite structure. The carbon fiber composite lay-up of $(45/90/-45/0)_s$ XFEM fracture simulation shows a significant result, wherein the failure strength renders 0.2% of difference compared with the experimental results (21.6%).

The good correlation of results in investigating the size effect modelling has been presented in this report. The results are in close agreement between the experimental and analytical data of each specimen modelled based on the size of the carbon fiber composite volume.

Acknowledgements

The authors gratefully acknowledge the support of Ministry of Education Malaysia and International Islamic University Malaysia.

References

[1] Sosa JC, Karapurath N. Delamination modelling of (glare) using the extended finite element method. Compos Sci Technol 2012;72(7):788 –91.

[2] Al-ansari LS, Al-mahmud HN, Al-raheem SK. Calculating stress intensity factor (mode i) for composite plate with central crack. Int J Comput Appl 2013;75(15):1–10.

[3] Lecheb S, Nour A, Chelli A, Mechakra H, Hamad N, Kebir H. Stress intensity factor for dynamic cracking of composite material by x-fem method. Int J Math, Comput, Phys, Electr Comput Eng 2014;8(5):809–15.

[4] Zhou LM, Meng GW, Li XL, Li F. Analysis of dynamic fracture parameters in functionally graded material plates with cracks by graded finite element method and virtual crack closure technique. Adv Mater Sci Eng 2016;.

[5] Belytschko T, Black T. Elastic crack growth in finite elements with minimal remeshing. Int J Numer Meth Eng 1999;45(5):601 –20.

[6] Golewski G, Golewski P, Sadowski T. Numerical modelling crack propagation under mode (ii) fracture in plain concretes containing siliceous fly-ash additive using (xfem) method. Comput Mater Sci 2012;62:75 –8.

[7] Huynh DBP, Belytschko T. The extended finite element method for fracture in composite materials. Int J Numer Meth Eng 2009;77(2):214–39.

[8] Moreno MS, Curiel-Sosa J, Navarro-Zafra J, Vicente JM, Cela JL. Crack propagation in a chopped glass-reinforced composite under biaxial testing by means of (xfem). Compos Struct 2015;119:264 –71.

[9] Navarro-Zafra J, Curiel-Sosa JL, Serna Moreno MC. Three-dimensional static and dynamic analysis of a composite cruciform structure subjected to biaxial loading: A discontinuum approach. Appl Compos Mater 2016;23(2):139–54.

[10] Grogan D, Brdaigh C, Leen S. A combined (xfem) and cohesive zone model for composite laminate microcracking and permeability. Compos Struct 2015;120:246 –61.

[11] Yazdani S, Rust WJ, Wriggers P. An (xfem) approach for modelling delamination in composite laminates. Compos Struct 2016;135:353 –64.

[12] Hu X, Chen B, Tirvaudey M, Tan V, Tay T. Integrated xfem-ce analysis of delamination migration in multi-directional composite laminates. Compos Part A: Appl Sci Manuf 2016;90:161 –73.

[13] Wang Z, Yu T, Bui TQ, Tanaka S, Zhang C, Hirose S, et al. 3-d local mesh refinement (xfem) with variable-node hexahedron elements for extraction of stress intensity factors of straight and curved planar cracks. Comput Meth Appl Mech Eng 2017;313:375 – 405.

[14] Hallett SR, Jiang WG, Khan B, Wisnom MR. Modelling the interaction between matrix cracks and delamination damage in scaled quasi-isotropic specimens. Compos Sci Technol 2008;68(1):80 –9.

[15] Mohammadi S. EXTENDED FINITE ELEMENT METHOD for Fracture Analysis of Structures. Blackwell Publishing Ltd; 2008. ISBN 978-1-4051-7060-4.

[16] Stolarska M, Chopp DL, Mos N, Belytschko T. Modelling crack growth by level sets in the extended finite element method. Int J Numer Meth Eng 2001;51(8):943–60.

[17] Nasr MN, Ng EG, Elbestawi M. A modified time-efficient {FE} approach for predicting machining-induced residual stresses. FE Anal Des 2008;44(4):149 –61.

[18] Rice J, Rosengren G. Plane strain deformation near a crack tip in a power-law hardening material. J Mech Phys Sol 1968;16(1):1 – 12.

[19] Jernkvist LO. Fracture of wood under mixed mode loading: I. derivation of fracture criteria. Eng Fract Mech 2001;68(5):549 –63.

[20] Wisnom M, Khan B, Hallett S. Size effects in unnotched tensile strength of unidirectional and quasi-isotropic carbon/epoxy composites. Compos Struct 2008;84(1):21 –8.

[21] Corum JM, Battiste RL, Liu KC, Ruggles MB. Basic properties of reference crossply carbon-fiber composite. Tech. Rep.; Lockheed Martin Energy Research Corporation; 2000.

[22] Pinho S, Robinson P, Iannucci L. Fracture toughness of the tensile and compressive fibre failure modes in laminated composites. Compos Sci Technol 2006;66(13):2069 –79.

[23] Ibtihal-Al-Namie , Ibrahim AA, Hassan MF. Study the mechanical properties of epoxy resin reinforced with silica (quartz) and alumina particles. Iraqi J Mech Mater Eng 2011;11(3):486 – 5069.